Investigation of Optimal Physical Parameters for Precise Proton Irradiation of Orthotopic Tumors in Small Animals

Marie Vanstalle, Julie Constanzo, Christian Finck

Accepted Manuscript

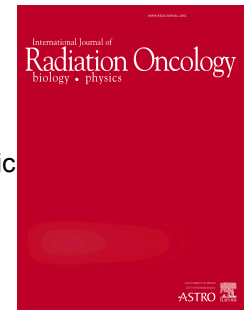

Investigation of optimal physical parameters for precise proton irradiation of orthotopic tumors in small animals

Marie Vanstalle, Julie Constanzo, Christian Finck

PII: S0360-3016(18)34041-0

DOI: https://doi.org/10.1016/j.ijrobp.2018.11.044

Reference: ROB 25416

To appear in: *International Journal of Radiation Oncology • Biology • Physics*

Received Date: 24 November 2017

Revised Date: 12 November 2018

Accepted Date: 26 November 2018

Please cite this article as: Vanstalle M, Constanzo J, Finck C, Investigation of optimal physical parameters for precise proton irradiation of orthotopic tumors in small animals, *International Journal of Radiation Oncology • Biology • Physics* (2019), doi: https://doi.org/10.1016/j.ijrobp.2018.11.044.

Investigation of optimal physical parameters for precise proton irradiation of orthotopic tumors in small animals

Short title: Optimal proton irradiation of small animal orthotopic tumors

Marie Vanstalle*, Julie Constanzo and Christian Finck
Université de Strasbourg, CNRS, IPHC UMR 7178, F-67000 Strasbourg, France

*Author to whom correspondence should be addressed.
Complete address:
Institut Pluridisciplinaire Hubert Curien
Département DRHIM
23 rue du Loess - BP 28
67037 Strasbourg cedex 2 (France)
Tel: +33 3 88 10 64 86
marie.vanstalle@iphc.cnrs.fr

Conflict of interest: none

Investigation of optimal physical parameters for precise proton irradiation of orthotopic tumors in small animals

Abstract

Purpose: The lack of evidence of biomarkers identifying patients that would benefit from proton therapy has driven the emergence of preclinical proton irradiation platforms using advanced small-animal models to mimic clinical therapeutic conditions. This study aims to determine the optimal physical parameters of the proton beam with a high radiation targeting accuracy, since small-animal tumors can reach millimetric dimensions at a maximum depth of about 2 cm.

Material and Methods: Several treatment plans, simulated using Geant4, were generated with different proton beam features to assess the optimal physical parameters for small volume irradiations. The quality of each treatment plan was estimated by dose-volume histograms and gamma index maps.

Results: Due to low energy straggling, low energy proton (<50 MeV) single-field irradiation can generate homogeneous SOBP to deliver a uniform dose in millimeter-sized tumors, while sparing healthy tissues located within or near the target volume. However, multi-field irradiation can limit the dose delivered in critical structures surrounding the target for attenuated high energy beams (E>160 MeV).

Conclusion: Low energy proton beam platforms are suitable for precision irradiation for translational radiobiology studies.

Keywords: Preclinical proton irradiation, targeted irradiation, dose accuracy, Geant4

Introduction

Despite its common use in the treatment of cancer, radiotherapy has only recently entered the era of precision medicine (1). A particularly exciting technology being currently explored for clinical applications is proton therapy (PT), which has the potential of higher dose conformity compared to photon beams, with less normal tissue being irradiated. However, the dose planning for PT is more complex than for conventional radiotherapy. A range error of even a few millimeters can lead to underdosage in the target volume and overdosage in the structures at risk (2–4). To date, a semi-personalized approach can be used with a reoptimization method based on linear energy transfer for intensity modulated PT, which is a safer treatment as it mitigates a potentially increased risk of side effects that result from the elevated relative biological effectiveness of proton beams near the end of the range (5). Recently, studies have focused on predicting patient-specific dosimetric benefits of PT (6) and dose escalation; for example, Chan *et al.* demonstrated low toxicity and high local control rate in patients with high-grade meningioma (7). Proton radiation dose escalation improved local control, but also increased toxicity (8). However, the inability to identify one or more biomarkers for conclusive patient outcomes limits the transfer of PT to personalized medicine. Therefore, small-animal proton irradiations are required to overcome these issues and refine the current guidelines. The use of proper animal models with human-like treatments is necessary to mimic the pathologies observed in patients. There is also a growing need to make progress in proton radiation biology – focused, for instance, on preclinical studies with linear energy transfer of clinical interest – in order to provide practicing radiation oncologists with accessible data. With burgeoning innovative preclinical irradiation techniques, new animal models of orthotopic xenografts have been developed, among others, for pancreatic (9) and lung cancer models (10). Precise irradiation platforms for preclinical studies were already developed with X-rays (11–13), and more recently, with protons (14–16). Through a common effort to improve dose delivery and treatment planning in small animals (17), radiation biological studies may easily be transferred to the clinic. This information will play a decisive role in proposing treatment and follow-up adapted to the characteristics of patients' tumors and individual radiosensitivity.

This study aims to define the optimal features of a proton beamline (energy, straggling, and beam size) required to accurately irradiate orthotopic xenograft tumors in small animals. Several geometries were considered with sizes comparable to brain and lung tumors in mice and rats (18). For each considered target volume, different Monte Carlo-based treatment plans were compared using proton energies and energy straggling corresponding to the existing preclinical facilities (14, 15, 19, 20). These features are proposed to optimize the design of subsequent preclinical studies.

Material and Methods

Setup geometry

The simulated geometric configuration was chosen to be similar to the existing preclinical setups (14, 19, 20). The water target corresponds to the irradiated volume. To obtain a passive modulated proton beam, a wheel with a set of attenuators of different thicknesses was placed before the target and after the beam exit to decrease the energy of the beam. Polyethylene material was chosen for beam attenuation, since it is commonly used for energy modulation. The uniformity of the beam profile after attenuation was achieved using aluminum collimators of various diameters (2 and 4 mm).

Two examples of orthotopic tumors with parallelepiped geometry, accounting for the typical size of mouse tumors (18, 21, 22), were chosen to assess the validity of the treatment plans:

- a $2\times2\times2$ mm^3 volume located at a depth of 4 mm in a water volume with a 0.3 mm thick compact bone at the beam entrance (corresponding to mouse skull thickness),
- a $4\times4\times4$ mm^3 volume located at a depth of 3 mm in a water volume with a 1 mm thick compact bone at the entrance (corresponding to rat skull thickness (23)),

For each tested tumor configuration, the prescribed dose was set to D_p=1 Gy.

Monte Carlo simulations

All results presented in this work were obtained using Monte Carlo simulations performed with Geant4 10.03 (24). Geant4 was chosen for its ability to simulate the nuclear reactions, which are not negligible at energies higher than 50 MeV. We used the Binary Cascade light ion model (BIC) to describe proton interactions. The BIC model, called *G4BinaryLightIonReaction*, was an extension of the binary cascade model described by Folger *et al*. (25). The pre-defined physics list *QGSP_BIC* was used in our study. In this model, the participating particles, i.e., primary particles or particles generated during the cascade process, are described by means of Gaussian wave functions. The electromagnetic physics list used was *G4EmStandardPhysics_option3*, which currently includes the ICRU 73 stopping power data up to 1 GeV/u (26). This physics list is recommended for hadrontherapy applications (27). The mean ionization potential in water was set to 79.2 eV corresponding to the average value previously reported (28). The step size was set to 0.1 mm, and the range cut to 1 mm (29).

Proton beam features

To determine the optimal proton features, several treatment plans were simulated based on available data with different proton beam energies (E) and energy straggling (σ_E) given at the beam exit, before modulation. The chosen features were the following:

- E=25 MeV, σ_E=0.127 MeV;
- E=30 MeV, σ_E=0.353 MeV;
- E=50 MeV, σ_E=0.500 MeV;
- E=68 MeV, σ_E=0.547 MeV;
- E=160 MeV, σ_E=0.855 MeV;
- E=200 MeV, σ_E=1.030 MeV.

These energies as well as their associated straggling correspond to existing facilities that can provide proton beam energies ranging from 25 MeV to 200 MeV (15, 30). It should be emphasized that, as the modulation of the beam was performed upstream the collimator and the phantom, the energy

straggling was considerably increased for higher energy beams. Additionally, three configurations were tested to assess the impact of multi-field irradiation on dose deposition:

- a single-field irradiation;
- a multi-field irradiation with three incidence angles of the beam at -45º, 0º, and +45º;
- a multi-field irradiation with five incidence angles of the beam at -45º, -25º, 0º, +25º, and +45º.

For each tumor geometry and physical beam features, a spread-out Bragg peak (SOBP) was built by superimposing several Bragg peaks of different energies obtained by modulating the initial beam with the attenuator wheel described above. For the mouse-type volume, the reference dose distribution comprised 12 proton energies between 19.72 MeV and 23.67 MeV with equally spaced energy levels, while it comprised 15 proton energies between 18.76 MeV and 28.37 MeV for the rat-type volume.

Assessment of the dose distributions

Cumulative dose volume histograms (DVH) (31) were used to assess the quality of the dose distribution and determine the minimal tumor size that could be homogeneously irradiated for a given energy (E_0 = 25, 30, 50, 68, 160, and 200 MeV) and straggling (σ_E) varying from 0 to 1 MeV. ICRU report 62 (32) stated that the acceptable dose heterogeneity (ΔD_M) is +7% to -5% of the prescribed dose in X radiotherapy. Therefore, the simulated target volume will be considered to be accurately irradiated when at least 100% of this volume received 95% of the prescribed dose (0.95 Gy in our case). An overdosage will be considered when the volume received more than 107% of the required dose (1.07 Gy in our case).

For each E_0 and σ_E, different SOBPs with a prescribed dose of 1 Gy were simulated with cubic target tumor sizes ranging from sub-millimeter to centimeter, and the corresponding DVH was then used to assess the homogeneity of the delivered dose. The smallest volume for which the simulated target was irradiated within the dose tolerance ΔD_M corresponds to the minimal tumor size that could be homogeneously irradiated with one field.

Gamma index

The gamma index (33, 34) directly compares the predicted with a reference dose distribution, accounting for the dose and spatial resolution. For each measured position $\vec{r}_m$, it is defined as (33, 35):

$$\gamma(\vec{r}_m) = min\sqrt{\frac{|\vec{r}_c, \vec{r}_m|^2}{DTA^2} + \frac{|D(\vec{r}_m) - D(\vec{r}_c)|^2}{\Delta D^2}}$$

where $\vec{r}_c$ is the reference position, $|\vec{r}_c, \vec{r}_m|$ the distance between the analyzed points, $|D(\vec{r}_m) - D(\vec{r}_c)|$ the dose difference, and *DTA* (distance-to-agreement) and ΔD the required accuracies for the distance and dose, respectively. In the following, the passing criteria were set at $\Delta D_M = ^{+7\%}_{-5\%}$, (32) and DTA=0.1, 0.2, or 0.3 mm, which respectively correspond to the ideal spatial dose resolutions for mouse, rat, and rabbit X-ray irradiations as recommended by Verhaegen *et al.* (32). These values should combine positioning, stability, and imaging precision. If the $\gamma(\vec{r}_m)$ value is less than 1, the calculation passes, and the delivered and predicted doses are considered to be in agreement. In our study, the gamma index was used only for single-field irradiation to assess the impact of the dose spatial resolution on the validity of the treatment plan.

A reference dose distribution, considered to be an optimal dose delivery to the target volume, was simulated using Geant4 for each considered geometry in order to calculate the gamma index. The simulated setup was the same as described in the *Setup geometry* section above using non-attenuated proton beam energies without energy straggling.

Results

Influence of energy straggling

Figure 1 shows the minimal tumor size that can be homogeneously irradiated with a single-field irradiation as a function of the initial proton beam energy spread. Tumor sizes less than 0.5 mm can be

homogeneously irradiated with proton beam energies less than 30 MeV and energy straggling less than 0.2 MeV. Higher energy beams attenuated at the beamline exit (160 and 200 MeV) cannot achieve homogeneous irradiation for volumes less than 1 cm^3 despite an energy straggling less than 0.2 MeV. This minimal size is constrained by the lateral scattering of the beam in the target.

Influence of beam modulation on stereotactic irradiations

Figure 2 compares the SOBP simulated using the initial beam features given in the *Proton beam features* section with the reference SOBP (black line) associated with the reference dose distribution defined in the *Material and Methods* section. The 2 mm (Fig. 2a) and 4 mm (Fig. 2b) volumes were irradiated with a single-field proton beam. At E=25 MeV with σ_E=0.127 MeV, the SOBP that targets the 2 mm volume (Fig. 2a) is homogeneous, similarly to the reference SOBP. This is not the case at higher energies, especially at 160 and 200 MeV, for which the important beam straggling generated by its modulation distorts the SOBP. It is noteworthy that the absorbed dose in the bone (e.g., skull) is about twice as high for high energy protons than for low energy ones, for which the absorbed dose in the bone insert is around 0.5 Gy (Fig. 2a).

A homogeneous SOBP is obtained with the 4 mm tumor volume at low energies (E=30 MeV; σ_E=0.353 MeV) (Fig. 2b). However, when the energy is increased to 50 and 68 MeV, the edge of the SOBP is shifted from 0.7 cm to 0.66 and 0.62 cm, respectively. At 160 and 200 MeV, the SOBP is a wide bump, with the maximal dose deposited immediately after the bone insert between 0.1 and 0.3 cm.

Influence of the spatial dose resolution

The gamma index maps calculated for each simulated configuration as well as the corresponding dose distributions are shown in Figures 3 and 4. Gamma index values corresponding to the 2 mm volume

irradiated with a 25 MeV beam (Fig. 3a) are always below 1 with a DTA of 0.1 mm. Conversely, deviations from the reference depth dose observed in Figure 2a are clearly visible when the energy is higher than 50 MeV. A gamma index close to 2 appears in the target volume at 50, 68, and 160 MeV for 0.1 mm DTA, which corresponds to an underdosage at the edge of the SOBP according to Figure 2. The gamma index values remain above 1 when increasing the DTA to 0.2 or 0.3 mm (Fig. 3d). Furthermore, when the energy is increased to 160 MeV, important areas with gamma index values of 2 appear before and after the tumor volume, demonstrating important discrepancies before and after the SOBP. This originates from the large spread of the SOBP due to the high attenuation of the proton beam.

For the 4 mm volume, the gamma index values are mainly below 1 in the target zone irradiated with a 30 MeV beam (Fig. 4a), although a region of higher gamma index values appears at the edge of the SOBP for a 0.1 mm DTA. Areas with gamma index values close to 2 appear at the distal edge of the target volume when the energy is up to 50 MeV (Fig. 4b). However, when the DTA is enlarged to 0.2 mm, corresponding to the spatial resolution required for rat irradiation, these areas fade to partially disappear with a 0.3 mm DTA. Conversely, for energies higher than 50 MeV (Fig. 4c-d), the gamma index values are close to 2 at the edges of the SOBP for all DTA values due to the important beam straggling generated by its modulation. Additionally, the overdosage in the bone insert highlighted above in Figure 2b for 160 MeV translates into high gamma index values.

Influence of the number of fields

Figure 5 presents the DVH for the treatment plans simulated with the six energies for the two target volumes with single-field irradiation (top panels). For both target volumes, protons of 25 MeV (2 mm volume) and 30 MeV (4 mm volume) achieve homogeneous irradiation within the required dose tolerance (indicated by the hashed area). At higher energies, an important part of the target volume receives a higher dose than the prescribed one. For example, at 200 MeV, 60% of the 4 mm volume receives 1.3 Gy. When the number of fields increases (middle and bottom panels, Fig. 5), the dose

uniformity in the target volume is improved for all energies. For the 2 mm volume, the dose delivered by the multi-field at 30 and 50 MeV beam energy is accurate within the dose tolerance for three fields. Even if the dose homogeneity is significantly enhanced at 160 and 200 MeV, an overdosage still remains in the target volume, although it is diminished compared to single-field irradiation. For example, 40% of the 4 mm volume receives more than 1.07 Gy using three radiation fields with the 200 MeV beam (Fig. 5b, bottom panel).

Figure 6 shows the DVH of the bone inserts associated with the dose delivery conditions used to produce the DVH in Figure 5. The dose delivered to the bone insert at the entrance of the target is always above 0.5 Gy in the 0.3 mm bone insert with a single radiation field (2 mm volume) as well as in the 1 mm insert (4 mm volume). Above 160 MeV, the bone insert receives more than 1 Gy. When the number of fields increases, the dose in the bone is drastically reduced, with 100% of both target volumes receiving between 0.15 and 0.5 Gy using five fields. Similarly to what is observed for single-field irradiation, medium beam energy (25-68 MeV) irradiations lead to a lower dose in the insert compared to energies above 160 MeV. However, this difference is highly attenuated by multi-field irradiations, with 100% of the bone receiving less than 0.3 Gy with five-field irradiation.

Discussion

The minimal volume size that can be irradiated in single-field irradiation is strongly dependent on the initial proton beam energy and its straggling (Fig. 1). For example, low energy beams (<50 MeV) can achieve homogeneous irradiation of volumes smaller than 2 mm. Of course, this minimal size has to be put into perspective with the maximum reachable depth. The irradiation of very small volumes (below 0.5 mm) is possible with low energy beams (25 and 30 MeV) and low energy straggling (σ_E<0.250 MeV), but is limited by the short proton range (~6.0 mm @25 MeV, ~8.0 mm @30 MeV). Consequently, the use of this energy range for preclinical irradiation should be limited to specific irradiations, such as mouse brain tumors that can be irradiated with 25 and 30 MeV beams.

Our results demonstrated that the uniform irradiation of very small volumes with attenuated high energy with a single radiation field cannot be achieved without an important over-irradiation of surrounding tissues. For example, according to the Figure 5a, more than 60% of the 2 mm volume receives more than 1.07 Gy when it is irradiated with a modulated beam above 50 MeV. Indeed, the energy straggling, which is usually proportional to the initial energy of the beam (36), is increased by the modulation, leading to a large SOBP spread (Fig. 2). For example, to decrease the proton energy from 160 MeV in order to irradiate a 4 mm volume, 16 cm of polyethylene is required, which increases the energy straggling by almost 4 MeV. This effect cannot be corrected by step-size variation in the modulation. Consequently, it will produce an overdosage in healthy tissues as well as part of the target volume. This outcome, highlighted by the DVH in Figures 5 and 6, was already pointed out by Ford *et al.* (15), who compared the depth dose profiles of a 30 MeV beam and modulated 100 MeV range-shifted beam in water. However, this effect can be significantly decreased, and the uniformity of the dose in the target volume can be improved by a multi-field proton beam (Fig. 5). Indeed, a homogeneous dose delivery in millimetric targets can be achieved by three-field irradiation with medium energy proton beams (< 68 MeV) (Fig. 5, bottom panel). Furthermore, the use of an energy selection magnet can significantly reduce the energy straggling of attenuated high energy beam. The lateral coverage can also be enhanced by enlarging the collimators size for higher energy beams, although it will result in an increase dose in surrounding tissues.

The choice of the optimal beam characteristics for small-animal proton irradiation also strongly depends on the required spatial resolution (given here by the DTA), which depends on the type of small animal to be irradiated. For example, the use of a 30 MeV single-field proton beam to irradiate a 2 mm volume is suitable when the DTA is increased from 0.1 mm to 0.2 mm (Fig. 3b). Similarly, the underdosage at the edge of the SOBP, observed for the target volume with a 50 MeV single-radiation field (Fig. 2), is attenuated when the DTA is increased (Fig. 4b).

Finally, it should be noted that the precise dose delivery in millimetric volumes is a technical challenge that requires very precise imaging (e.g., micro-CT scan, MRI (18)) and positioning systems. Several image-guided X-ray irradiation platforms that already exist for small animals can perform irradiations of millimetric orthotopic tumor volumes, such as mouse lung tumors that can reach 1 mm

in size, with a precision of 0.1 mm or less (21, 37, 38). To perform inter-comparisons between proton and X-ray treatments, similar irradiation accuracies between both modalities should be achieved, as proposed by Ford *et al.* (15).

Conclusion

This work demonstrated that low energy proton beams (E<68 MeV) are appropriate to carry out homogeneous irradiation of millimeter-sized tumors while sparing healthy tissues in preclinical studies. On the one hand, 25-30 MeV beams are suitable for mouse irradiations, as tumor dimensions in mice can be sub-millimetric, although low energies have a limited penetration depth of about 6-8 mm. On the other hand, a 50 MeV beam is more adapted to rat irradiation, as the organs are larger than in mice, thus providing greater flexibility for the choice of orthotopic model and dose accuracy. The use of attenuated high energy proton beams to irradiate small tumor volumes (< 1 cm) can be considered with a multi-field configuration. However, our results demonstrate that the important energy straggling of an attenuated high energy proton beam leads to a substantial overdosage in healthy tissues.

References

1. Baumann M, Krause M, Overgaard J, *et al.* Radiation oncology in the era of precision medicine. *Nat. Rev. Cancer*. 2016;16:234–249.
2. Paganetti H. Range uncertainties in proton therapy and the role of Monte Carlo simulations. *Phys. Med. Biol.* 2012;57:R99-117.
3. Woodward WA, Amos RA. Proton Radiation Biology Considerations for Radiation Oncologists. *Int. J. Radiat. Oncol. Biol. Phys.* 2016;95:59–61.
4. McGowan SE, Burnet NG, Lomax AJ. Treatment planning optimisation in proton therapy. *Br. J. Radiol.* 2013;86:20120288.
5. Unkelbach J, Botas P, Giantsoudi D, *et al.* Reoptimization of Intensity Modulated Proton Therapy Plans Based on Linear Energy Transfer. *Int. J. Radiat. Oncol. Biol. Phys.* 2016;96:1097–1106.
6. Hall DC, Trofimov AV, Winey BA, *et al.* Predicting Patient-specific Dosimetric Benefits of Proton Therapy for Skull-base Tumors Using a Geometric Knowledge-based Method. *Int. J. Radiat. Oncol. Biol. Phys.* 2017;97:1087–1094.
7. Chan AW, Bernstein KD, Adams JA, *et al.* Dose Escalation with Proton Radiation Therapy for High-Grade Meningiomas. *Technol. Cancer Res. Treat.* 2012;11:607–614.
8. Liu H, Chang JY. Proton therapy in clinical practice. *Chin. J. Cancer*. 2011;30:315–326.
9. Tuli R, Surmak A, Reyes J, *et al.* Development of a Novel Preclinical Pancreatic Cancer Research Model: Bioluminescence Image-Guided Focal Irradiation and Tumor Monitoring of Orthotopic Xenografts. *Transl. Oncol.* 2012;5:77–84.
10. Saha D, Watkins L, Yin Y, *et al.* An Orthotopic Lung Tumor Model for Image-Guided Microirradiation in Rats. *Radiat. Res.* 2010;174:62–71.
11. Wong J, Armour E, Kazanzides P, *et al.* High-resolution, small animal radiation research platform with x-ray tomographic guidance capabilities. *Int. J. Radiat. Oncol. Biol. Phys.* 2008;71:1591–1599.
12. Verhaegen F, Granton P, Tryggestad E. Small animal radiotherapy research platforms. *Phys. Med. Biol.* 2011;56:R55-83.
13. Butterworth KT, Prise KM, Verhaegen F. Small animal image-guided radiotherapy: status, considerations and potential for translational impact. *Br. J. Radiol.* 2015;88:20140634.
14. Greubel C, Assmann W, Burgdorf C, *et al.* Scanning irradiation device for mice in vivo with pulsed and continuous proton beams. *Radiat. Environ. Biophys.* 2011;50:339–344.
15. Ford E, Emery R, Huff D, *et al.* An image-guided precision proton radiation platform for preclinical in vivo research. *Phys. Med. Biol.* 2017;62:43.
16. Meyer J, Stewart RD, Smith D, *et al.* Biological and dosimetric characterisation of spatially fractionated proton minibeams. *Phys. Med. Biol.* 2017.
17. Vanstalle M, Constanzo J, Karakaya Y, *et al.* Analytical dose modelling for preclinical proton irradiation of millimetric targets. *Med. Phys.* 2017.
18. Wang F, Akashi K, Murakami Y, *et al.* Detection of Lung Tumors in Mice Using a 1-Tesla Compact Magnetic Resonance Imaging System. *PLoS ONE*. 2014;9.
19. Russo G, Pisciotta P, Cirrone GAP, *et al.* Preliminary study for small animal preclinical hadrontherapy facility. *Nucl. Instrum. Methods Phys. Res. Sect. Accel. Spectrometers Detect. Assoc. Equip.* 2017;846:126–134.
20. Takata T, Kondo N, Sakurai Y, *et al.* Localized dose delivering by ion beam irradiation for experimental trial of establishing brain necrosis model. *Appl. Radiat. Isot.* 2015;105:32–34.
21. Motomura AR, Bazalova M, Zhou H, *et al.* Investigation of the effects of treatment planning variables in small animal radiotherapy dose distributions. *Med. Phys.* 2010;37:590–599.

22. Mathieu D, Lecomte R, Tsanaclis AM, *et al.* Standardization and detailed characterization of the syngeneic Fischer/F98 glioma model. *Can. J. Neurol. Sci. J. Can. Sci. Neurol.* 2007;34:296–306.
23. Nowak K, Mix E, Gimsa J, *et al.* Optimizing a rodent model of Parkinson's disease for exploring the effects and mechanisms of deep brain stimulation. *Park. Dis.* 2011;2011:414682.
24. Agostinelli S, Allison J, Amako K, *et al.* Geant4—a simulation toolkit. *Nucl. Instrum. Methods Phys. Res. Sect. Accel. Spectrometers Detect. Assoc. Equip.* 2003;506:250–303.
25. Folger G, Ivanchenko VN, Wellisch JP. The Binary Cascade: Nucleon nuclear reactions. *Eur. Phys. J. A.* 2004;21:407–417.
26. Ivanchenko V, Apostolakis J, Bagulya A, *et al.* Recent Improvements in Geant4 Electromagnetic Physics Models and Interfaces. *Prog. Nucl. Sci. Technol.* 2011;2:898–903.
27. Lechner A, Ivanchenko VN, Knobloch J. Validation of recent Geant4 physics models for application in carbon ion therapy. *Nucl. Instrum. Methods Phys. Res. Sect. B Beam Interact. Mater. At.* 2010;268:2343–2354.
28. Paul H. On the Accuracy of Stopping Power Codes and Ion Ranges Used for Hadron Therapy. In: *Advances in Quantum Chemistry*.Vol 65. Elsevier; 2013:39–61.
29. Grevillot L, Frisson T, Zahra N, *et al.* Optimization of GEANT4 settings for Proton Pencil Beam Scanning simulations using GATE. *Nucl. Instrum. Methods Phys. Res. Sect. B Beam Interact. Mater. At.* 2010;268:3295–3305.
30. Ulmer W, Schaffner B. Foundation of an analytical proton beamlet model for inclusion in a general proton dose calculation system. *Radiat. Phys. Chem.* 2011;80:378–389.
31. Drzymala RE, Mohan R, Brewster L, *et al.* Dose-volume histograms. *Int. J. Radiat. Oncol. Biol. Phys.* 1991;21:71–78.
32. International Commission on Radiation Units and Measurements. *Prescribing, Recording and Reporting Photon Beam Therapy*. 1999.
33. Low DA, Harms WB, Mutic S, *et al.* A technique for the quantitative evaluation of dose distributions. *Med. Phys.* 1998;25:656–661.
34. Depuydt T, Van Esch A, Huyskens DP. A quantitative evaluation of IMRT dose distributions: refinement and clinical assessment of the gamma evaluation. *Radiother. Oncol.* 2002;62:309–319.
35. Winiecki J, Morgaś T, Majewska K, *et al.* The gamma evaluation method as a routine QA procedure of IMRT. *Rep. Pract. Oncol. Radiother.* 2009;14:162–168.
36. Paganetti H, Jiang H, Parodi K, *et al.* Clinical implementation of full Monte Carlo dose calculation in proton beam therapy. *Phys. Med. Biol.* 2008;53:4825–4853.
37. Song KH, Pidikiti R, Stojadinovic S, *et al.* An x-ray image guidance system for small animal stereotactic irradiation. *Phys. Med. Biol.* 2010;55:7345–7362.
38. Zhou H, Rodriguez M, van den Haak F, *et al.* Development of a micro-computed tomography-based image-guided conformal radiotherapy system for small animals. *Int. J. Radiat. Oncol. Biol. Phys.* 2010;78:297–305.

Figure captions

FIGURE 1. Minimal cubic tumor size that can be irradiated with different proton energies as a function of the initial energy straggling of the beam. The points corresponding to the nominal features of the proton beams described in this work (see *Proton beam features* section) are indicated by squares (15, 30). Points are connected to lines to guide the eye.

FIGURE 2. Comparison between simulated SOBPs obtained for a 2 mm tumor (a) and 4 mm tumor (b), irradiated with proton beams of 25 (only for the 2 mm tumor), 30, 50, 68, 160, and 200 MeV. *Reference* corresponds to non-attenuated proton beam energies without energy straggling (black line). The dose discontinuity at the entrance of the target corresponds to the proton interaction in the bone insert.

FIGURE 3. Dose distributions and gamma index maps for the treatment plans generated to irradiate the 2 mm volume with a 0.1 mm DTA, with proton beams of 25 (a), 30 (b), 50 (c), 68 (d), and 160 MeV (e). The target volume is indicated by the white box. The gamma index maps generated with a DTA of 0.2 and 0.3 mm are presented in the insert boxes.

FIGURE 4. Dose distributions and gamma index maps for the treatment plans simulated to irradiate the 4 mm volume with a 0.1 mm DTA, with proton beams of 30 (a), 50 (b), 68 (c), and 160 MeV (d). The target volume is indicated by the white box. The gamma index maps generated with a DTA of 0.2 and 0.3 mm are presented in the insert boxes.

FIGURE 5. Comparison of the DVH of the target volumes obtained for the treatment plans of the 2 mm volume (a) and 4 mm volume (b) irradiated with 25 (in the case of the 2 mm volume alone), 30, 50, 68, 160, and 200 MeV. The middle panel shows DVHs obtained for three radiation fields, and the bottom panel for five radiation fields. The hashed area indicates the accepted dose tolerance around

the 1 Gy prescribed dose. The DVH were normalized to a common point (requiring 100% of the volume receiving 0.95 Gy) for comparative purposes.

FIGURE 6. Comparison of the DVH of the bone inserts obtained for the treatment plans of the 2 mm volume (a) and 4 mm volume (b) irradiated with 25 (in the case of the 2 mm volume alone), 30, 50, 68, 160, and 200 MeV. The middle panel shows the DVH obtained for three radiation fields, and the bottom panel for five radiation fields.

Formatting of funding sources

This research did not receive any specific grant from funding agencies in the public, commercial, or not-for-profit sectors.

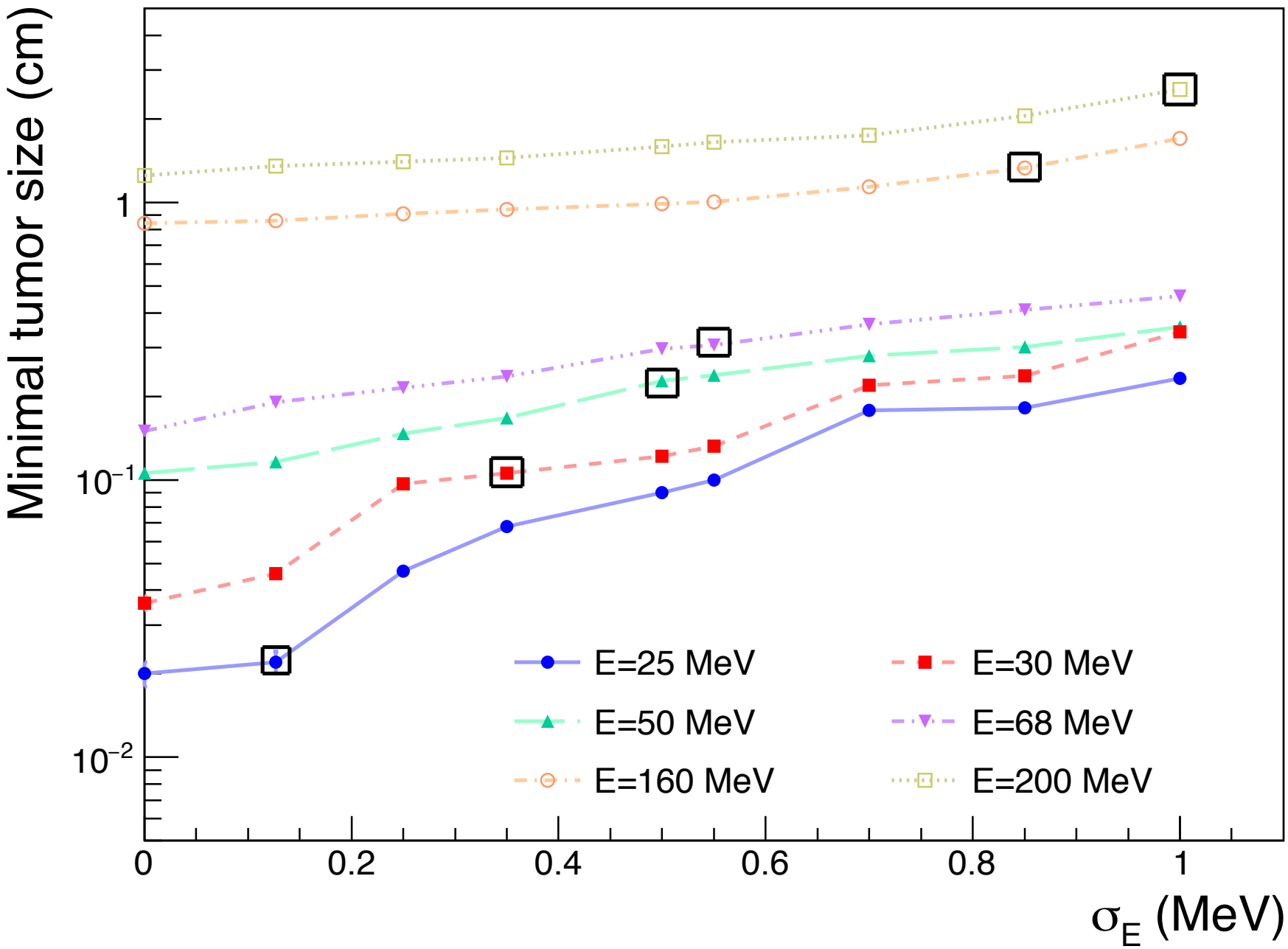
Minimal tumor size (cm)
1
10^{-1}
10^{-2}
0
0.2
0.4
0.6
0.8
1
σ_E (MeV)
E=25 MeV
E=30 MeV
E=50 MeV
E=68 MeV
E=160 MeV
E=200 MeV

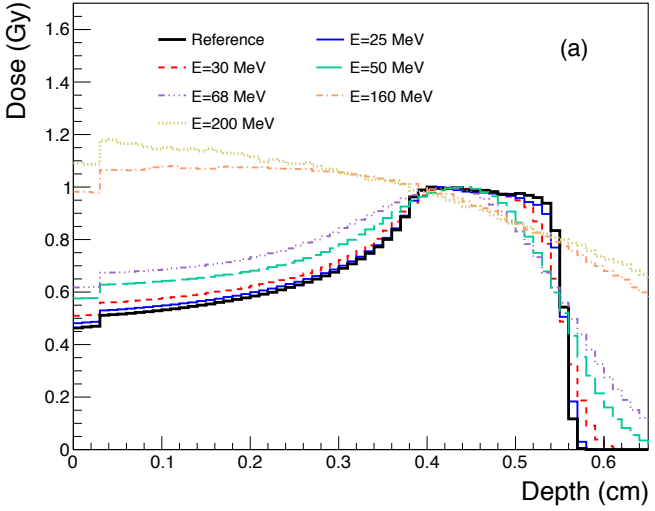

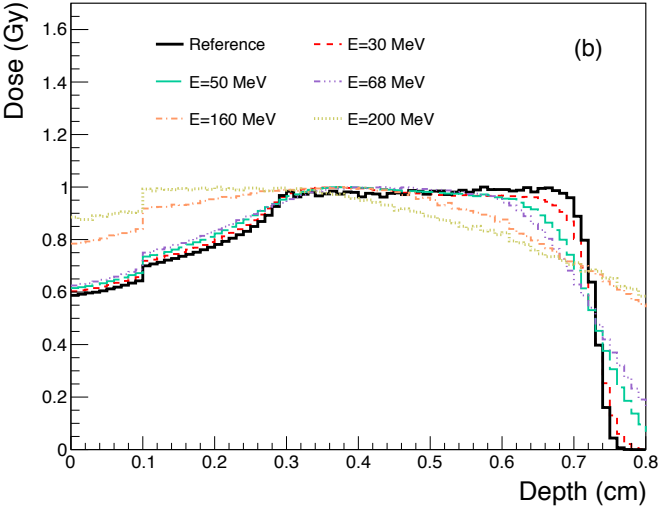

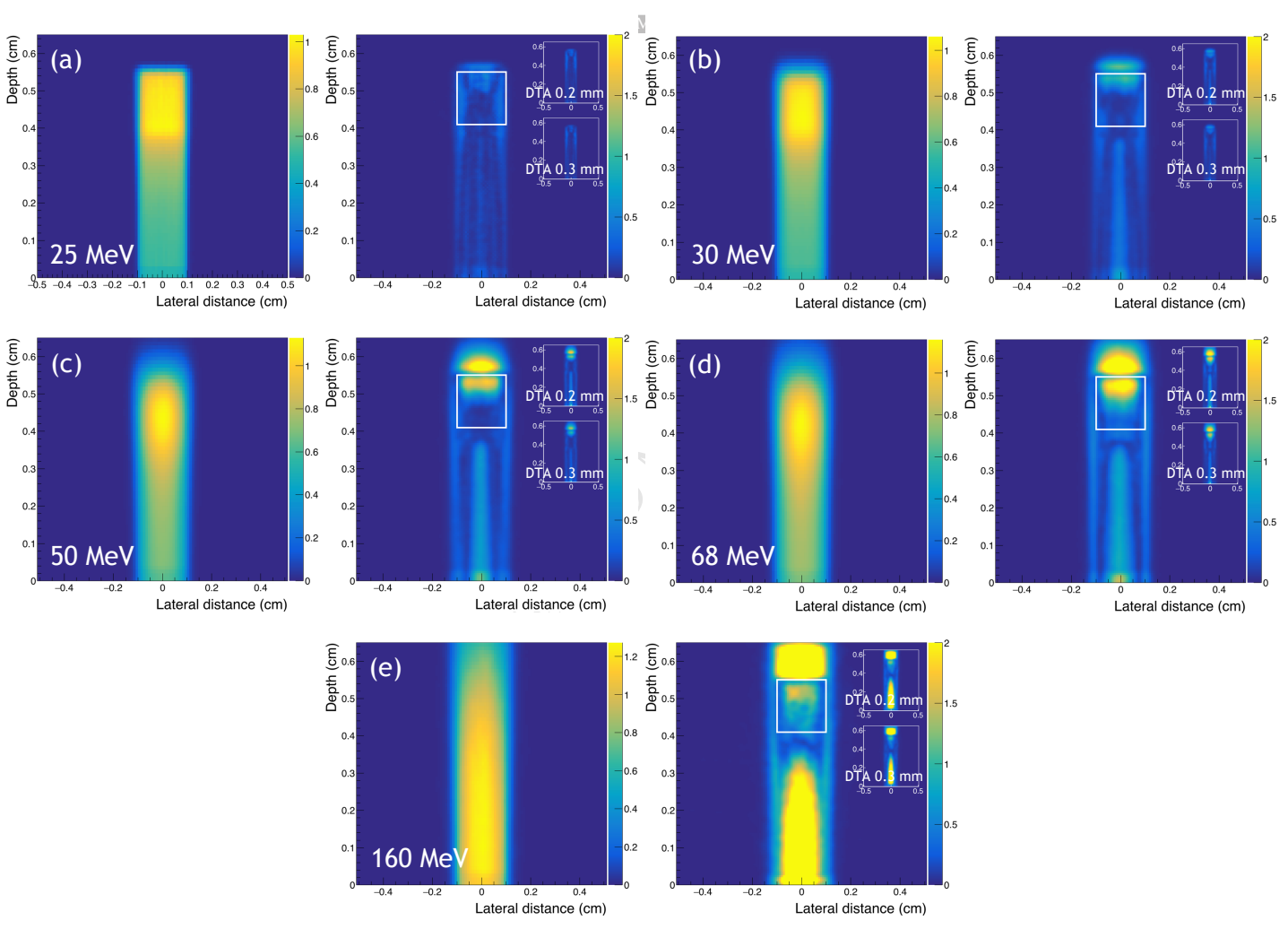
(a)
25 MeV
(b)
30 MeV
(c)
50 MeV
(d)
68 MeV
(e)
160 MeV
DTA 0.2 mm
DTA 0.3 mm
Depth (cm)
Lateral distance (cm)

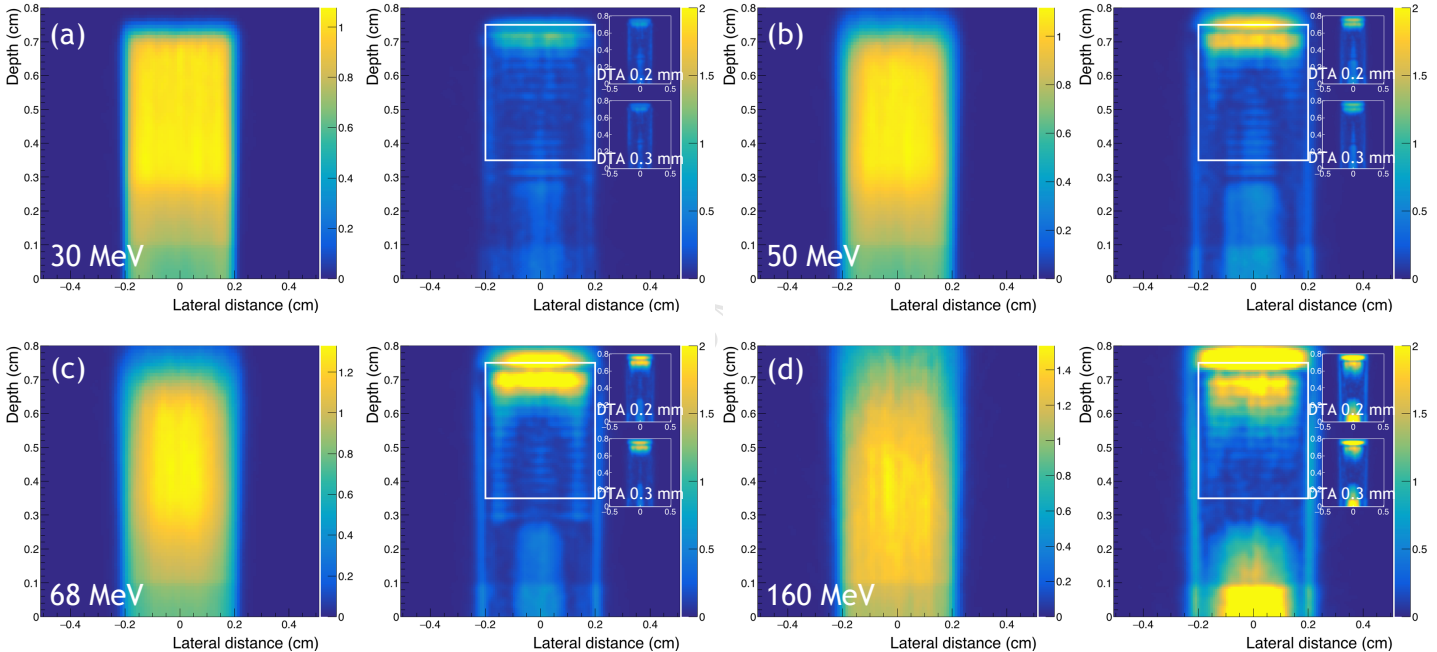
(a)
30 MeV
(b)
50 MeV
(c)
68 MeV
(d)
160 MeV
DTA 0.2 mm
DTA 0.3 mm
Depth (cm)
Lateral distance (cm)

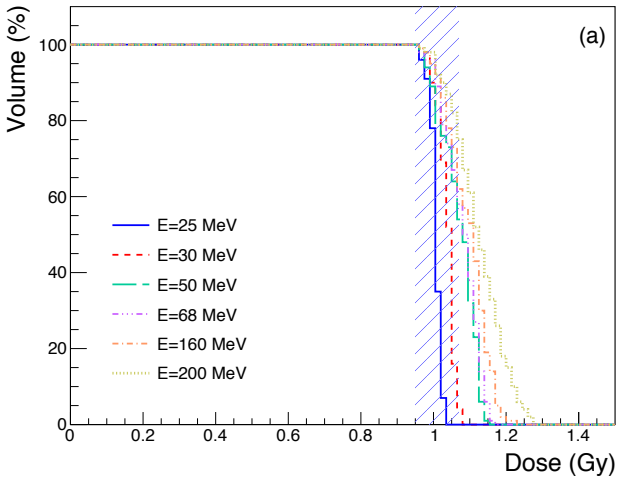
(a)
Volume (%)
Dose (Gy)
E=25 MeV
E=30 MeV
E=50 MeV
E=68 MeV
E=160 MeV
E=200 MeV

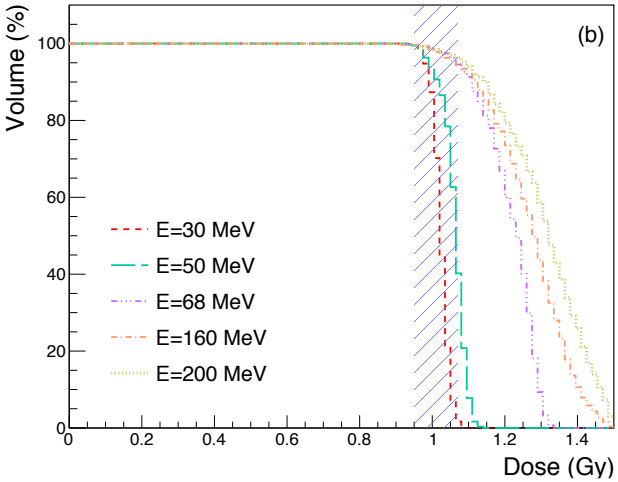
(b)
Volume (%)
Dose (Gy)
E=30 MeV
E=50 MeV
E=68 MeV
E=160 MeV
E=200 MeV

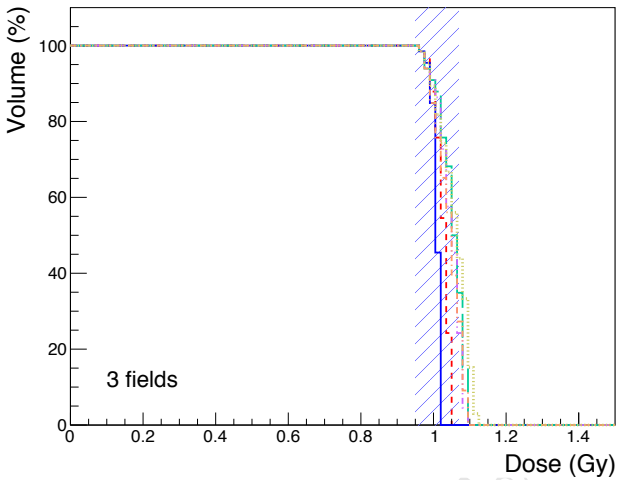
Volume (%)
Dose (Gy)
3 fields

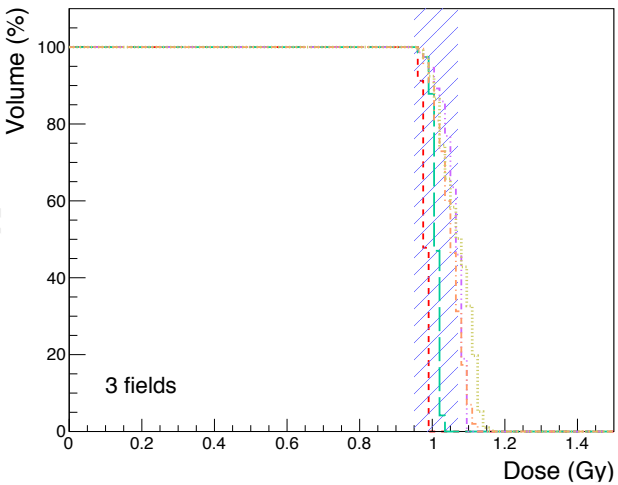
Volume (%)
Dose (Gy)
3 fields

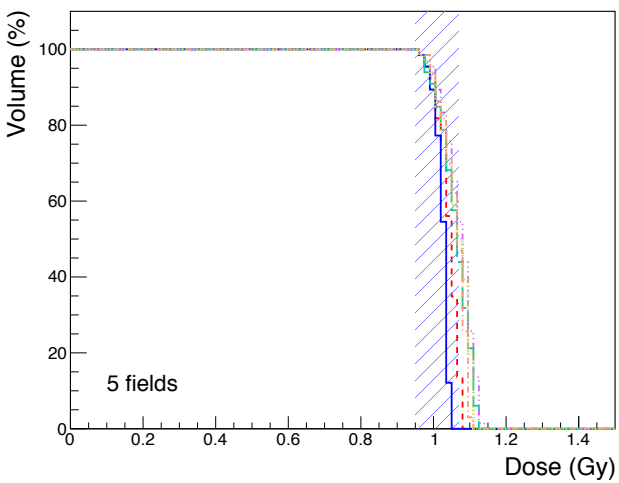
Volume (%)
Dose (Gy)
5 fields

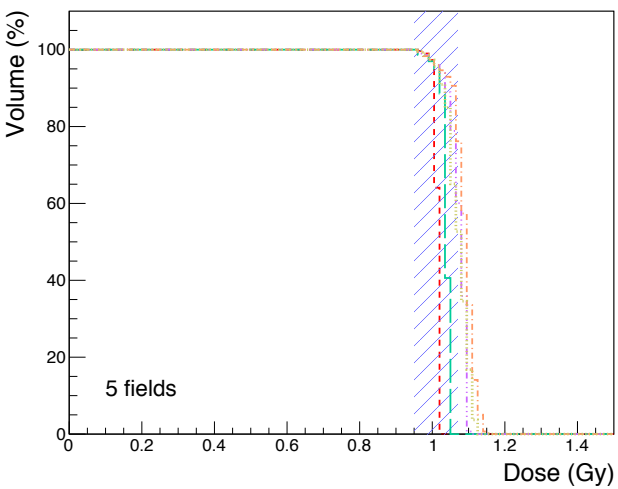
Volume (%)
Dose (Gy)
5 fields

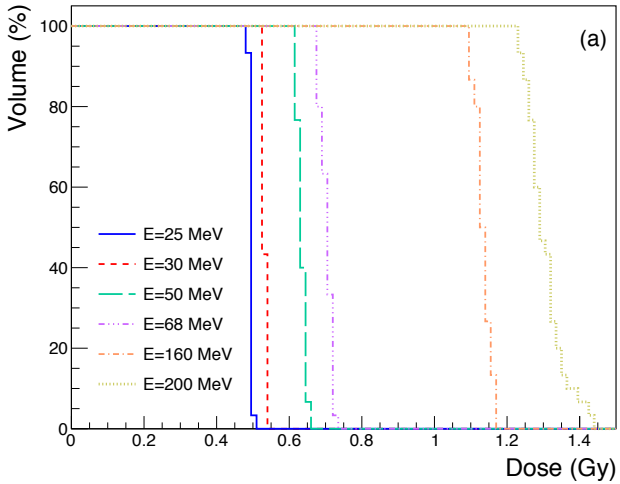
(a)
Volume (%)
Dose (Gy)
E=25 MeV
E=30 MeV
E=50 MeV
E=68 MeV
E=160 MeV
E=200 MeV

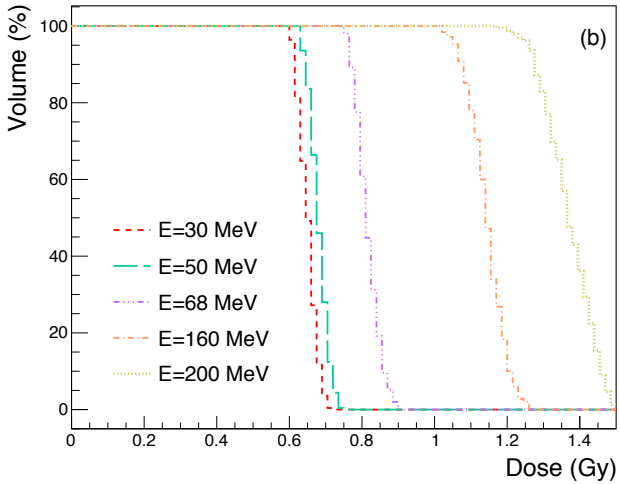
(b)
Volume (%)
Dose (Gy)
E=30 MeV
E=50 MeV
E=68 MeV
E=160 MeV
E=200 MeV

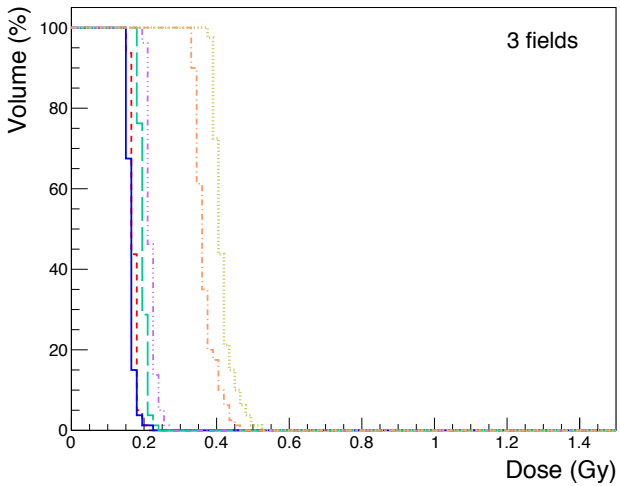
3 fields
Volume (%)
Dose (Gy)

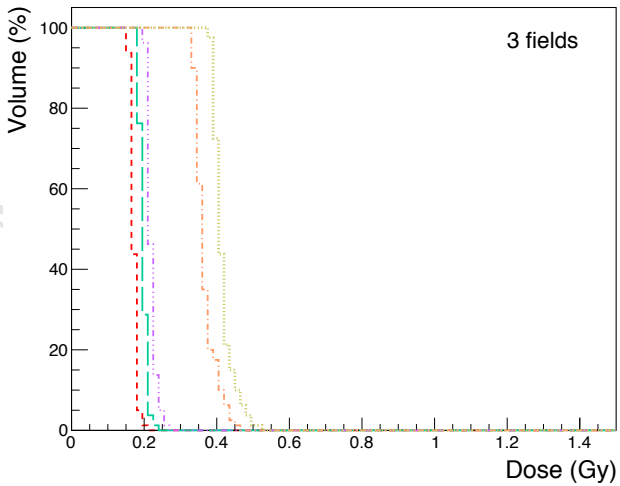
3 fields
Volume (%)
Dose (Gy)

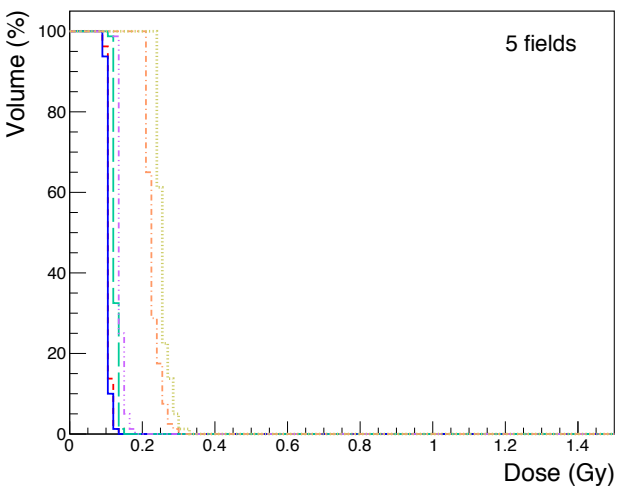
5 fields
Volume (%)
Dose (Gy)

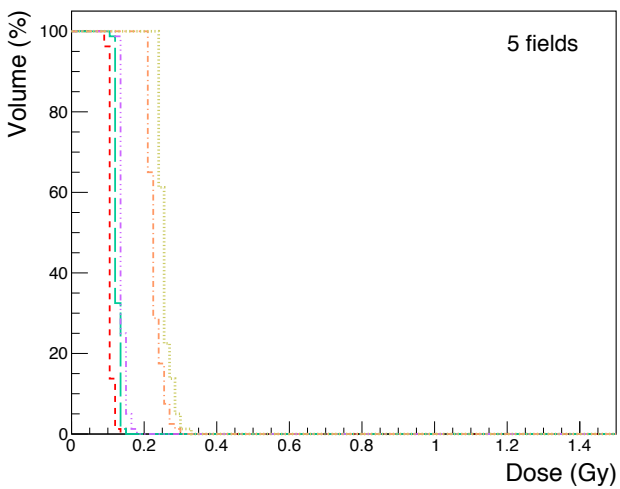
5 fields
Volume (%)
Dose (Gy)

Investigation of optimal physical parameters for precise proton irradiation of orthotopic tumors in small animals

Summary

The emergence of preclinical proton irradiation platforms dedicated to radiobiological studies drives the development of small-animal models, mimicking clinical therapy conditions.

Targeted irradiations of small volumes are conditioned by the proton beam physical properties. Based on available proton beam data and Geant4 simulations, the optimal features to correctly deliver the prescribed physical dose in small-animal tumors were determined. In particular cases of millimetric tumors, low energy protons are better suited than protons > 50 MeV.